20-Industrial Crystallography

MS-20.01.07 THE USE OF DYNAMIC AND STRUCTURAL CRYSTALLOGRAPHIC TECHNIQUES TO STUDY THE SYNTHESIS OF ZIRCONIA. By Xavier Turrillas, Industrial Materials Group, Crystallography Dept. Birkbeck College (University of London), Malet Street, LONDON WC1E 7HX, U.K.

There is a considerable research effort in the engineering of zirconia ceramics. This is due to its current applications and potential uses in other fields (fuel cells for instance). The results presented here are part of a collaborative project between Industry and University and illustrate how the facilities and analytical techniques only available from *big science* institutions, can be used in the solution of narrowly defined technological problems.

In this work we are presenting our contributions to the understanding of how the oxide crystallization from the hydroxide precursor takes place, and how the transition, at higher temperatures, between the tetragonal and monoclinic phases occurs.In particular, we have focused our attention on the influence of the preparation pH of the hydroxide. In order to achieve this, we have used real time analytical techniques, such as time-resolved Synchrotron Energy Dispersive Diffraction and Neutron Thermo-Diffractometry (NTD). As a complement to determine the local zirconium hydroxide structure, synchrotron extended X-ray absorption fine structure (EXAFS) techniques at room temperatures were also employed as well. Different thermal treatments (heating and cooling ramps and dwelling times) were applied to various samples in order to examine their influence on the crystallites' size and the tetragonal-monoclinic transition temperature. The influence of the preparation pH on the temperature of the cystallization from the hydroxide has been measured using conventional X-ray and neutron diffraction techniques and Energy dispersive diffraction.

The influence of thermal treatment on the tetragonal-monoclinic transition temperature is more complicated but clear trends of behaviour have emerged from the experimental data. Briefly, the higher the dwelling temperature and times, the higher is the transition temperature. On the other hand, the specimens prepared at low pH are more sensitive to heat treatment. Another observation reported by other authors concerning the relation between crystallite size and the tetragonal-monoclinic transformation temperature has also been confirmed here. Regarding the crystallization from the hydroxide, it seems to occur at least in three stages. A careful analysis of the NTD integrated profiles, by fitting to a tentative theoretical model suggests that the first stage is related to the removal of terminal OH^-/H_2O-groups of the hydroxide, whereas inner-water removal and oxolation (two hydroxide bonds reduced to one oxo-bond and free water) are involved in the two subsequent stages.

MS-20.01.08 STRUCTURAL FEATURES OF POROUS SILICON WITH VISIBLE PHOTOLUMINESCENCE. By Osamu Nittono*, Kuniko Takemoto and Yoshio Nakamura, Department of Metallurgy, Tokyo Institute of Technology, 2-12-1 Oh-okayama, Meguro-ku, Tokyo 152, Japan.

It has been reported that porous silicon (PS) has wirelike (or columnar) structures of less than 10nm in diameter and that the effective photoluminescence is due to a quantum size effect resulting from such isolated fine rods. The size and morphology of such PS, however, is strongly related with the dopant type and content (or resistivity) as well as preparation conditions such as current density and HF concentration (H.Sugiyama and O.Nittono, J. Cryst. Growth, 1990, 103, 156-163). In order to understand the mechanism of this phenomenon, it is first necessary to examine the photoluminescene of porous Si in relation to the real microstrucutre of PS. Therefore, in this study the microstructure, morphology, size, lattice expansion and crystallinity of PS's, which were formed on p-type and n-type degenerate Si(100) substrates of less than 0.02 Ω cm resistivity, were studied by means of high resolution scanning microscopy, X-ray multi-crystal diffractometry, high resolution electron microscopy. Anodization was carried out with current densities ranging from 10 to 300 mA/cm^2 in a constant electrolyte of $HF:C_2H_5OH:H_2O=1:2:1$ with the reaction time from 15 to 30 min. All the n-type PS's were prepared under illumination by a 100W halogen lamp. The emission of visible photoluminescence was checked by a He-Cd laser beam (325nm); luminescent color varied from yellow to orange according to preparation conditions.
The main results are as follows: (1) p-type PS: PS showed color changes from bluish-gray to dark golden brown with increasing the porosity. When PS was prepared above 250 mA/cm^2, the lattice distortion decreased and thus the crystallinity was considerably worse than that of the substrate, and visible luminescence was appreciated. PS, which is composed of large pores, showed slightly larger lattice distortions than PS, composed of small pores: the smaller in diameter the remaining Si rods were, the larger the lattice distortion was. This was also confirmed by investigating X-ray intensity distribution around the reciprocal lattice point for PS, indicating that the lattice relaxation easily takes place with decreasing the mean radius of the remaining Si rods. The remaining Si rods were found to be composed of particlelike strucutre of various sizes from several nm to several tens of nm (a kind of mosaic structure), probably as a result of stress relaxation of the remaining Si rods in PS layer.
(2) n-type PS: Characteristics of the crystallinity and morphology of PS were quite different from those of the p-type PS. Illumination was found to be very effective in producing PS on n-type Si substrates. From structural observations of PS's prepared by varying the reaction time in a range from 1 s to 15 min., it was revealed that the microstructure of PS, when produced for a long reaction time, was composed of mainly three layers which exhibit different pore morphology; a spongy structure, composed of fine Si particles, in the upper region near the surface, a dendritic one in the middle region, and a cylindrical one in the lower region near the interface between PS and Si substrate. The depth profiles measured by a heavy-ion ERD (Elastic Recoil Detection) spectrometer for PS's emitting strong photoluminescence showed that hydrogen atoms were densely concentrated near the upper surface of the PS layer, even after being annealed at 900℃ in dry nitrogen ambient. This result suggests that the origin of the photoluminescence is related to the existence of hydrogen atoms near the PS surfaces.

PS-20.01.09 PHASE IDENTIFICATION IN STEEL BY ELECTRON MICROSCOPY
*Ping Liu Dept. of Physical Metallurgy, Research & Development Centre AB Sandvik Steel S-811 81 Sandviken Sweden

The advantage of electron microscopy over x-ray is the ability to relate the structure to the morphology and chemistry in a very small area in steel. The composition of a given phase varies depending upon the alloy composition and thermal mechanical treatment. Therefore, electron diffraction is the only reliable way to identify a phase. Because of the three dimensional information in the convergent beam electron diffraction (CBED) only one pattern from high-symmetry zone axis may be needed for phase identification (J.W.Steeds & R.Vincent, J.Appl.Cryst.1983, 16, 317-324).
Both carbides $M_{23}C_6$ and M_6C have FCC structure with a= 10.6-11.2 Å. But they belong to different space groups: $Fm\bar{3}m$ for $M_{23}C_6$and $Fd\bar{3}m$ for M_6C. The mesh sizes are the same both in the zero-order Laue zone (ZOLZ) and the first-order Laue zone (FOLZ) in the CBED pattern of [001] zone axis from $M_{23}C_6$ (Fig.1). By contrast the mesh size in the ZOLZ of the same zone axis from M_6C is as twice large as in the FOLZ due to the distinction of h00, $h\neq 4n$ type reflections in the ZOLZ (Fig.2). Hence, $M_{23}C_6$ and M_6C can readily be distinguished.
CBED patterns from [001] zone axes of σ-phase ($P4_2/mnm$, a=8.79 Å c=4.54 Å), π-phase ($P4_132$, a=6.47 Å) and χ-phase ($I\bar{4}3m$, a=8.8037 Å) are shown in Figs. 3, 4, and 5 respectively. The mesh sizes in the ZOLZ are very similar for all three patterns(Note that the camera lengths are different in Figs.3-5). There are no

displacements between ZOLZ and FOLZ for σ-phase and π-phase. Morever, the radii of the FOLZ rings in Figs 3, 4 and 5 reveal that c=4.54 Å and a=6.47 Å and a=8.8037 Å for σ-phase, π-phase and χ-phase respectively.

M_7C_3 has the space group Pnma with a= 4.526 Å, b=7.010 Å and c= 12.142 Å. Its pseudo-hexagonal [100] axis pattern in Fig.6 shows similar spacings in comparison with the pattern from the [0001] zone of R-phase ($R\bar{3}$, a=10.903 Å and c=19.342 Å) in Fig.7. However, the radii of the FOLZ rings are very different, which give a=4.526 Å for M_7C_3 and c=19.345 Å for R-phase respectively.

Because of the very long c-axis of μ-phase ($R\bar{3}m$, a=4.754 Å and c=25.71 Å) the pattern of [0001] has a distinctive feature: small radius for the FOLZ ring and several higher order Laue zones may appear (Fig.8) .

Figs.1-8. CBED patterns. **Figs.1-5.** The [001] zone axes of $M_{23}C_6$, M_6C, σ-, π- and χ-phase respectively. **Figs.6-7.** The [100] and [0001] zone axes of M_7C_3 and R-phase respectively. **Fig.8.** The [0001] zone axis of μ-phase.

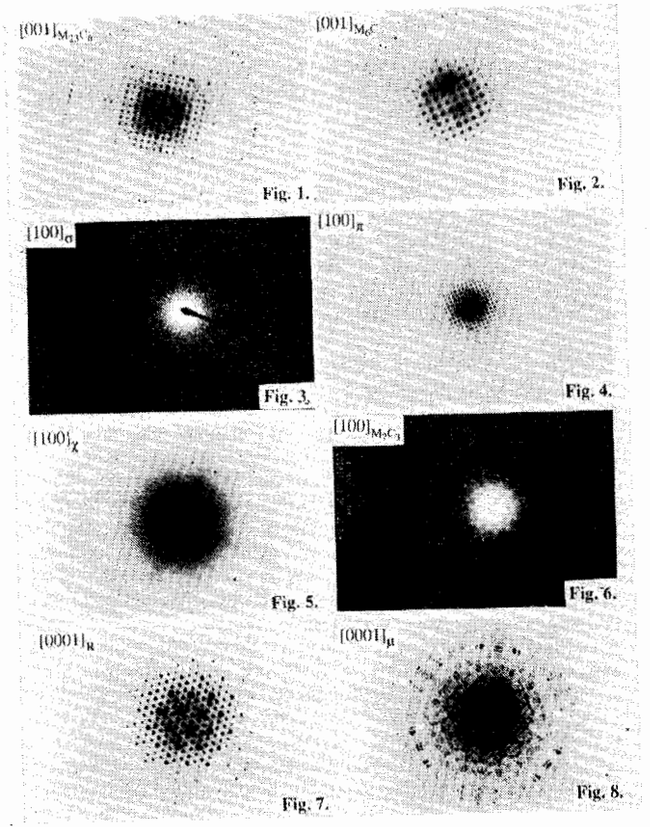

electrolysis (Zhang, 1990), the extracted powder is obtained from the alloy and examined by XRD. The figure below shows the XRD pattern which contains the so-called W and Z phase (Padezhnova et al., 1982) peaks. However, detailed examinations by conventional selected area diffraction (SAD), convergent beam diffraction (CBD) and energy dispersive spectrum (EDS) analysis show that the icosahedral quasicrystal (QC), $MgZn_2$-type Laves phase, W phase and an ordered structure of W phase (W′ phase) are present. It is clearly that the distinct XRD peaks from the Z phase in the XRD pattern are in fact coincident with those peaks from the icosahedral QC and $MgZn_2$-type Laves phase, as listed in the table below. The XRD peaks from the QC in rapidly solidified Mg-Al-Zn alloy (Rajasekhara, 1986) are given out for comparison. It is necessary to point out that the QC in the Mg-Zn-Y system has never been reported before.

Table Indexing of the XRD Peaks from the Z Phase

Exper.		indexing		Z phase		QC-MgAlZn	
d(nm)	I/I_o	QC	Laves	d(nm)	I/I_o	d(nm)	I/I_o
0.2455	53	(100000)		0.245	50	0.2423	51
0.2328	100	(110000)		0.234	100	0.2292	100
0.2267	24		(021)	0.225	12		
0.2182	13		(004)	0.217	7		
0.2061	32	(111101)		0.206	33	0.2032	23
0.198	13		(113)	0.1985	16		
0.1449	21	(101000)		0.1442	30	0.1428	19

Padezhnova E M et al. (1979). Akademiia Nauk SSSR, Izvestiia, Metally, No.4, 204-208 (in Russian)
Zhang S Q (1990). Acta Metall. Sinica, **3**, 110-115
Rajasekharan T et al. (1986), Nature, **322**, 528-530

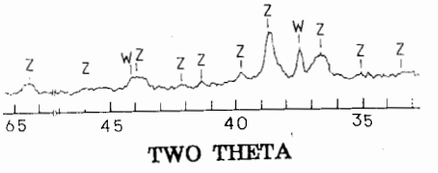

PS-20.01.10 STUDY OF Z PHASE IN MB25 Mg ALLOY. By Z.P. Luo* and S.Q. Zhang, Institue of Aeronautical Materials, Beijing 10095, P.R. of China.

The microstructures of Mg-Zn-Y system alloys were studied by Padezhnova et al. (1982). By means of x-ray diffraction (XRD) analysis, a Z phase was identified in this system alloys, but its crystallographic structure was not determined out. The present paper gives the results of study on the structure of the so-called Z phase in literature.

The experimental material is as-cast MB25 alloy with compositions of 5.56～5.78 wt-%Zn, 0.47～0.6 wt-%Zr, 0.89～1.72 wt-%Y and balanced Mg. By means of

PS-20.01.11 THE STRUCTURAL REARRANGEMENT ASSOCIATED WITH LITHIUM INSERTION INTO V_6O_{13}. By C. Lampe-Önnerud * and J.O. Thomas, Uppsala University, Institute of Chemistry, Box 531, S-751 21 Uppsala, Sweden.

In spite of the fact that V_6O_{13} is one of the most common cathode materials used in modern battery design, the structural mechanisms of lithium insertion are still not properly understood. Conventional wisdom says that phases $Li_xV_6O_{13}$, where x=1, 4 and 8, are created successively on lithium insertion. It is known, however, that difficulties can arise with respect to battery reliability and reproducibility. These may well result from difficulties incurred in obtaining